Operation Method Study Based on the Energy Balance of an Independent Microgrid Using Solar-powered Water Electrolyzer and an Electric Heat Pump

Shin'ya Obara

Power Engineering Laboratory, Department of Electrical and Electronic Engineering, Kitami Institute of Technology

165 Koen-cho, Kitami, Hokkaido 090-8507, Japan

E-mail: obara@mail.kitami-it.ac.jp

Phone and FAX : +81-157-26-9262

Seizi Watanabe

Department of Mechanical Engineering, Kushiro National College of Technology

Otanozhike 2-32-1, Kushiro, Kokkaido 084-0916, Japan

E-mail: seiji@mech.kushiro-ct.ac.jp

Phone: +81-154-57-7298

Fax : +81-154-57-5360

Balaji Rengarajan

Centre for Fuel Cell Technology, International Advanced Research Centre for Powder Metallurgy and New Materials,India

IIT-M Research Park, Phase-1, Second Floor, 6, Kanagam Road, Taramani, Chennai 600 113, India

E-mail: balaji.energy@gmail.com

Phone: +91-44-66632708

Abstract

A completely energy-independent microgrid (green microgrid) was examined in this work with the aims of abating greenhouse gas emissions by spreading the use of green energy, providing energy backup systems for disaster, and increasing the energy utilization efficiency with the use of exhaust heat. This paper analyzed the energy supply to six houses in a cold region. The green microgrid consisted of photovoltaics, water electrolyzers, proton-exchange membrane fuel cells (PEFCs), and

heat pumps. To investigate the operation method and the capacity of each piece of equipment in the arrangement, a distributed system with two or more sets of equipment and a central system with one set of equipment were analyzed by a genetic algorithm. By introducing the prior energy need pattern of a cold region into the proposed system, the operation method and equipment capacity based on the power and heat balance were clarified. By introducing the partial load performance of a water electrolyzer and a PEFC into the analysis program, the operation method of each system was investigated. It was found that the area of a solar cell of a distributed system could be reduced by 12% as compared to a central system.

Abbreviations

COP: Coefficient of performance

GA: Genetic algorithm

PEFC: Proton-exchange membrane fuel cell

1. Introduction

The use of green energy to reduce greenhouse gas can be achieved by introducing an energy system based on microgrids. The introduction of a microgrid is also expected to contribute to the reduction of greenhouse gases. Furthermore, a microgrid can be used to distribute power for a backup energy supply in the case of a widespread disaster. However, the introduction of unstable green energy into small-scale electric power grids requires many studies to guarantee the quality of the electric power. Therefore, there have been many investigations of microgrid technology with the operation, scheduling and control [1-6]. Furthermore, design and optimization of a microgrid are also investigated widely [7-17]. To fully utilize the unstable green energy from a microgrid, hydrogen and oxygen for the fuel cells can be introduced by a water electrolyzer and a gas storage unit consisting of a compressor and a tank, for example. Complex systems of photovoltaics and water electrolyzers have also been constructed and investigated in the past [18-28]. In this paper, an energy-independent green microgrid consisting of a water electrolyzer operating with the electric power of photovoltaics, a fuel cell, and a heat pump is proposed. In this case, one must clarify the

quality of the electric power (the range of fluctuation of the frequency and voltage) of an optimized green microgrid based on the electric power and the thermal energy income and output along with the transient response characteristic of the electric power. This paper describes the optimization of a green microgrid based on the electric power and thermal energy balance. Because the fuel cell, the water electrolyzer, and the heat pump introduced into the system all have nonlinear characteristics, a genetic algorithm (GA) was used for the optimization process. Moreover, the algorithm assumed that the proposed system was installed in a house in a cold region with a high demand for thermal energy.

The electricity and thermal energy demands of the entire proposed microgrid were satisfied using the electric power obtained from two or more photovoltaics. The surplus power from the photovoltaics was distributed to the water electrolyzers to produce hydrogen and oxygen. The electricity demand was satisfied by distributing these stored hydrogen and oxygen gases to PEFCs in case the power could not be provided by the photovoltaics. By using the output characteristics of the actual equipment, the partial load performance of the green microgrid was investigated. Different partial load performances were observed between the two types of systems because the load factors and arrangement of each piece of equipment in a distributed system with the same capacity differed from those of a central system with one set of equipment. In addition, the individual capacity of the solar cell, the fuel cell, the water electrolyzer, and the heat pump used in the green microgrid was verified.

2. Green microgrid

2.1 Basic configuration of the proposed microgrid

Figure 1 shows the basic configuration of the proposed microgrid, which consisted of a power network, a heat network, a hydrogen network, and an oxygen network. Houses A, B, and C were connected to the microgrid, each with different equipment. The power network was used to transfer electric power to each house. The heat network transmitted heat to each house using hot water. A network of hydrogen and oxygen was used to supply the hydrogen and oxygen produced by the water electrolyzers to each fuel cell.

A heat storage tank and a heat pump were installed in House A, and high temperatures could be supplied to the heat network. A PEFC was installed in House B, and the electric power and exhaust heat were supplied to their respective networks. A solar cell, water electrolyzer, and hydrogen and oxygen compressors and cylinders were installed in House C. The surplus power of the solar cell, the hydrogen and the oxygen were supplied to each network from House C.

2.2 System outline

Figure 2 is a system flow chart of a green microgrid with water electrolyzer using solar energy. The electric power and heat were supplied to six houses in the microgrid, as shown in Figure 2. The electric power generated in the photovoltaics (photovoltaics (1) to (3)) was provided to the electric power supply of the grid, the heat pumps (heat pumps (1) and (2)), and the water electrolyzers (water electrolyzers (1) to (3)). In this work, both the central system, which had one set of large-scale equipment, and the distributed system, which consisted of two or more sets of equipment with smaller capacities, were investigated. The hydrogen and oxygen generated by the water electrolyzers were stored in their respective cylinders using compressors, and the gases could be supplied to the PEFCs (fuel cells (1) to (3)) at an arbitrary time. The total capacity was shared equally among the PEFCs and the water electrolyzers in a distributed system. On the other hand, the central system had one fuel cell and one water electrolyzer.

Figure 2 (b) shows the heat supply system. The exhaust heat of the PEFCs was stored in a heat storage tank through the heat network. When the heat demand of the microgrid exceeded the amount of heat stored, the additional required heat was supplied by the heat pump.

2.3 Energy balance of the system

Equations (1) and (2) are the balance equations of the electric power and the heat energy of the microgrid shown in Fig. 2. The left-hand and right-hand sides of each equation are the input and output terms, respectively. $E_{needs,t}$ and $H_{needs,t}$ of the right-hand side of each equation are the electricity and thermal demand. The subscript t for each equation is the sampling time. One set of equipment including fuel cells, photovoltaics, a water electrolyzer, and a heat pump are

configurable in the central system ($N_{FC} = N_{PV} = N_{EL} = N_{HP} = 1$), and two or more sets of the same components are configurable in the distributed system ($N_{FC} > 1$, $N_{PV} > 1$, $N_{EL} > 1$, $N_{HP} > 1$). Furthermore, hydrogen and oxygen compressors (E_{CP}) used in water electrolyzer and a blower (E_{BW}) were taken into consideration as auxiliary machines consuming power. The air blower was used for the PEFC cathode and for cooling the water electrolyzer. The mechanical power of a hot water pump circulating in the microgrid was not included in Eq. (1). However, the loss accompanying the heat input and output of the heat storage tank was taken into consideration. Therefore, the terms for heat input efficiency ($\eta_{HST,in}$) and heat output efficiency ($\eta_{HST,out}$) of the heat storage tank were included in Eq. (2).

2.4 Equipment characteristics

(1) Fuel cell

Figure 3 (a) shows the performance of a home PEFC cogeneration unit with a 1-kW output reported by Tokyo Gas of Japan [29, 30]. The efficiency of the fuel reformer was subtracted from the total power generation efficiency of the system to obtain the curve of the electrical energy output and the PEFC thermal power in Fig. 3 (a). As shown in the figure, the difference between the maximum and minimum power generation efficiency in the partial load operation of the PEFC without a reformer was approximately 10%. When the output characteristics of the electric power and the heat from the PEFCs were approximated with a curve, Eqs. (3) and (4) were obtained.

(2) Water electrolyzer

In this paper, hydrogen was assumed to be generated by the proton-exchange membrane method developed by Rengarajan et al. [31]. Figure 3 (b) shows the experimental results of the load factor L_f and H_2 production efficiency η_{EL} of the hydrogen generator described above [31]. Equations (5) and (6) define the potential efficiency η_{ELe} and the current efficiency η_{ELi}, respectively, and the energy efficiency η_{EL} can be calculated by Eq. (7). As shown in Fig. 3 (b), the maximum efficiency at the time of low hydrogen loading exceeded 90%. On the other hand, the production efficiency of H_2 at the time of the maximum load was approximately 70%. Thus, the efficiency

decreased as the load factor increased, and the characteristics for the water electrolyzer differed greatly from those of the fuel cell. Equation (8) was obtained when the relationship between the load factor shown in Fig. 3 (b) and the H_2 production efficiency was approximated with a curve. The performance of the water electrolyzer was obtained by introducing this approximation into the analysis described later.

(3) Hydrogen and oxygen gas compressor

The hydrogen and oxygen produced by the water electrolyzer were pressurized with compressors and stored in cylinders. The hydrogen and oxygen gases were assumed to be ideal gases, and the work done by the compressors at this time was calculated using Eq. (9). The term η_{CP} in the equation is the overall efficiency of the compressor. The power consumption in the inverter and motor, the transfer loss of the mechanical power, air leak, the loss from insufficient cooling, and other mechanical losses are included in η_{CP}. The value of η_{CP} was assumed to be 0.6 (60%) for a real system in the later analysis.

3. Operation Optimization Using a GA

3.1 Chromosome model

The output term of the fuel cell and the power input term of the water electrolyzer in the balance equation (Eq. (1)) are expressed by Eqs. (10) and (11), respectively. In the example of this paper, the fuel cell and the water electrolyzer were distributed and introduced into three sets equipment at the maximum. The terms α, β and χ of Eq. (10) and ξ, ψ and ζ of Eq. (11) are the load rates of the distributed fuel cells and the power input rate of the distributed water electrolyzers. Therefore, the total of α_t, β_t and χ_t at sampling time t and the total of ξ_t, ψ_t and ζ_t are both 1, as shown in Eqs. (12) and (13).

The chromosome model used for the GA expresses each value of α_t, β_t and χ_t, and ξ_t, ψ_t and ζ_t with a 0 or 1 (16 bits) generated at random for each sampling interval. Therefore, if the load rates of the fuel cells and the power input rates of the water electrolyzers of all the sampling times ($t = 0, 1, 2, \ldots 23$) were given, the operation method in the representative fuel cells and water electrolyzers would be determined. The chromosome model indicating the operation method of the

fuel cells and water electrolyzers in a typical day was defined as an individual in the GA. Figure 4 shows the configuration of the chromosome model used in this paper. The squares and the broken lines in Fig. 4 represent the composition chromosome model of an individual. To maintain the diversity of the chromosome group, the number of individual N_{cr} were handled by the same analysis in the GA.

Adapting of GA to a nonlinear problem is very easy. It is thought that optimization of a microgrid with various nonlinear equipment can be performed by introducing equipment characteristics as shown in Fig. 3, and the chromosome model shown in Fig. 4.

3.2 Analysis conditions

(1) Energy-need patterns

In this paper, the energy-loading patterns shown in Fig. 5 were used [32]. The load pattern of the electric power and the heat shown in Fig. 5 is the average value of a typical day for each month in a standard house in Sapporo, Japan. Electric lights and household appliances were included in the power load. On the other hand, the load for space heating and water heating, such as the hot water of a bathtub, was included in the thermal load.

(2) Meteorological condition of photovoltaics

Figure 6 (a) shows the outside air temperature of Sapporo on a typical day for each month in 2008 published by the Japan Meteorological Agency [33]. The difference between the mean temperature of a typical month and the mean temperature of the representative day in Fig. 6 was set as the smallest temperature difference. Figure 6 (b) shows the amount of insolation received for a sloped surface on a representative day for each month, as described above [34]. The insolation of the sloped surface was calculated as the amount of insolation incident on a board inclined at an angle of 30 degrees in the southern direction.

The production of electricity by the solar cell introduced into the microgrid was obtained by multiplying the amount of insolation on the sloped surface shown in Fig. 6 (b) by the area of the solar cell and the power generation efficiency. Figure 7 shows the integrated value of the amount of insolation on a representative day for each month shown in Fig. 6 (b).

(3) COP of a heat pump and outside air temperatures

Figure 8 shows the relationship between the load factor of the heat pump using air as a heat source and the coefficient of performance (COP) introduced into the microgrid. It also shows the performance of a standard heat pump. The COP of the heat pump is dependent on the outside air temperature, as shown in Fig. 6 (a). Figure 8 shows that the COP of the heat pump fell rapidly for load factors lower than 60%. An approximate expression of the load factor and COP for the case of an outside air temperature of 16 °C is shown in Eq. (14). Similar to Eq. (14), an approximate expression for the COP of a heat pump was prepared for each given outside air temperature. The COP of a heat pump for each sampling time in a representative day is obtained from the approximate expressions of COP at a given outside air temperature.

(4) Composition of a green microgrid

The central system was composed of one set of equipment, which included a fuel cell, a photovoltaic, a water electrolyzer, and a heat pump. On the other hand, the distributed system consisted of three sets of fuel cells, three sets of photovoltaics, three sets of electrolytic cells, and two sets of heat pumps. Electric power and heat were supplied to six individual houses from the microgrid. The pieces of equipment shown in Fig. 1 were either centralized or distributed in each house. Table 1 shows the outline, efficiency, and power consumption of each piece of equipment used for analysis.

3.3 System operation and the required amount of energy

Table 2 shows the relationship between the system condition and the input/output of electric power and heat at sampling time t based on the energy balance Eqs. (1) and (2). After the electric power of the photovoltaics was supplied to the power conditioner (a DC-DC converter and an inverter), it was supplied to the heat pump to fulfill the electricity and thermal demands. The surplus power in this case was used to produce hydrogen and oxygen using a water electrolyzer. The electricity produced by the photovoltaics was used to supply the stored hydrogen and oxygen to the PEFCs when the electric power of photovoltaics is less than demand. Although the exhaust heat of

the PEFCs in this case was used to satisfy the thermal demand, the excess heat was stored in a heat storage tank.

Because hydrogen, oxygen, and heat storage tanks were installed in the proposed system, it was necessary to operate the system based on the amount of hydrogen ($Q_{H_2,ST,t-1}$) and heat ($H_{HST,t-1}$) stored at sampling time $t-1$ such that the energy balance Eqs. (1) and (2) could be satisfied. The initiation of the system operation ($t=0$) changes the initial conditions, such as the energy demand, the electric energy of the photovoltaics, and the quantity of hydrogen, oxygen, and heat stored. Therefore, in this study, the start of system operation was taken to be 0:00 ($t=0$), and the amount of residual hydrogen at the end of a representative day ($t=23$) was planned so that it would exceed the amount of hydrogen required for the start of operation ($t=0$) for the next day.

3.4 Objective function

The amount of hydrogen stored at the beginning of operation ($t=0$) and the end ($t=23$) of the day was $Q_{H_2,ST,0}$ and $Q_{H_2,ST,23}$, respectively. Equation (15) is the objective function of the proposed system. When the operation of the proposed microgrid was determined based on Eq. (15), the system consumed the minimum amount of hydrogen and oxygen at the equipment capacity with the chosen operation method.

3.5 Analysis flow

Figure 9 shows the analysis flow of the optimization process of the proposed system by the GA. First, after inputting the analysis conditions such as the area of the solar cells and the solution parameters of the GA, many chromosome models, as described in Fig. 4, were generated at random in a computer. The power output ($E_{FC,i,t}$) of each PEFC and the power input ($E_{EL,l,t}$) of each water electrolyzer at sampling time t were determined by decoding these chromosome models and assigning values of α_t, β_t and χ_t, and ξ_t, ψ_t and ζ_t to Eqs. (7) and (8). When the power output of each PEFC was determined, the load factor of the fuel cell was used in Eq. (4). Subsequently, the $H_{FC,t}$ of the PEFC exhaust heat at time t could be obtained from the set

capacity of the fuel cell. When $H_{FC,t}$, the heat demand ($H_{needs,t}$) and the amount of heat storage($H_{HST,t-1}$) at time $t-1$ were assigned to Eq. (2), the thermal power $H_{HP,j,t}$ for the heat pump was obtained. The load factor of the heat pump was calculated using $H_{HP,j,t}$ as described above and the capacity of the heat pump. The value of COP was determined from the relationship of the load factor, the outside air temperature, and Fig. 8. The power consumption $E_{HP,t}$ of the heat pump was obtained from the COP. The amount of energy stored by the hydrogen and oxygen $Q_{H_2,ST,t}$ could be obtained by using the following quantities in Eq. (1): the electricity $E_{PV,j,t}$ produced by the photovoltaics obtained from Fig. 6 (b), the power demand $E_{needs,t}$, the power consumption $E_{EL,l,t}$ of each water electrolyzer, the power consumption $E_{CP,m,t}$ of the compressor for compressing the hydrogen and oxygen (obtained by water electrolyzer using surplus power), and the power consumption $E_{BW,n,t}$ of the blower.

As shown in Fig. 9, the same number of chromosome models and operation methods were planned. The populations that fit the objective function (Eq. (15)) from these operation plans were arranged. To maintain the diversity of these populations, cross-over genetic manipulation and mutation were added to the probability beforehand to the population with a high ranking. The solution to the final generation was defined as the optimal solution.

Using the operation optimization program displayed in Fig. 9, the minimal solar cell area, the amount of hydrogen initially stored, the capacity of the heat pump, the capacity of the fuel cell, and the capacity of the water electrolyzer were calculated as shown in Fig. 10. From the minimization analysis of the capacity of each piece of equipment, as described above, the optimal solution was obtained by changing the equipment capacity given to the program in small increments. The capacitance of the fuel cell and the water electrolyzer in the distributed system was equal. Moreover, the relationship of the load factor and the efficiency of the fuel cell and the water electrolyzer followed Figs. 3 (a) and 3 (b) without being dependent on the capacity of each piece of equipment.

3.6 Determination of equipment capacity

The optimal solution of the system operation for each month was obtained by introducing the load pattern of the average electric power and heat shown in Fig. 5 into the energy balance Eqs. (1) and (2) using the meteorological conditions of a representative day for each month, as shown in Fig. 6. However, the capacity of each piece of equipment did not change from month to month. Therefore, the components of the system were determined by choosing the largest capacities of each piece of equipment over one year.

4. Analysis Results

4.1 Optimal capacity of each component

Figure 11 shows the analysis results of the optimized fuel cell, the water electrolyzer, and the amount of hydrogen stored in the system at the beginning of operation ($t = 0$), which is described as the amount of initial hydrogen storage. Figure 12 shows the analysis results of the optimized area of the solar cell and the capacity of the heat pump. As shown in Fig. 11 (a), there was almost no difference between the capacities of the fuel cell in the distributed system and the central system. Figures 11 (b) and 11 (c) show that the difference between the two systems was larger after September due to the capacity of the water electrolyzer and the initial hydrogen storage. This occurred because the integrated amounts of insolation on a representative day for each month of the mid-term (from March to May) of the first half of year and the mid-term of the second half of year (from September to November) were significantly different, as shown in Fig. 7. During the mid-term operation of the second half with less insolation, more power was supplied from the fuel cell. Therefore, the system with the water electrolyzer and the fuel cell operated significantly differently water electrolyzer between the mid-term of the first half of year and the mid-term of the second half of year. The reason for the significantly different amounts of initial hydrogen storage between the distributed system and the central system (Fig. 11 (c)) is as follows: the area of the total solar cell for the period of the mid-term of the second half to winter was because the distributed system was smaller than the central system, as shown in Fig. 12 (a). Therefore, a distributed system would be more suitable during these months due to the higher operation efficiency as compared to a central system. Moreover, because there was no difference between the capacity of the fuel cell in either

system, as shown in Fig. 11 (a). Furthermore, the capacity of the water electrolyzer of the distributed system may be smaller than that of the central system in the mid-term from September to November, as shown in Fig. 11 (b). Therefore, the load factor of the water electrolyzer of the distributed system in this period may be larger as compared to that of the central system. As a result, the efficiency of the water electrolyzer from September to November decreased.

On the other hand, the analysis results of the capacity of the heat pump changed very little between the central system and the distributed system, as shown in Fig. 12 (b).

4.2 Average operation efficiency of the fuel cell and the water electrolyzer

Figure 13 shows the results of the average operation efficiency for a representative day of the fuel cell and the water electrolyzer. The average operating efficiency in Fig. 13 was obtained by summing the efficiency at each sampling time (except at the end of the operation) of the fuel cell and the water electrolyzer for one day and dividing the totals by each hour of operation. The efficiency of the fuel cell of the distributed system during the summer season was high compared to the central system, as shown in Fig. 13. This was because the load factor of the fuel cell was low in the summer season as the heat pump consumed less power. Therefore, the fuel cell of the distributed system could operate with a higher power generation efficiency as compared to the central system with a large capacity.

4.3 Seasonal differences in operation methods

Figures 14 and 15 show the analysis results of the operating efficiency of the fuel cell and the water electrolyzer and the heat pump COP of the distributed system and the central system for each sampling time for a representative day in February and August. Because the amounts of heat demanded in February and August differed greatly, the capacities of the heat pumps were also significantly different, as shown in Fig. 12 (b). As a result, the efficiency of the fuel cell at partial load operation dropped frequently, as shown in Figs. 14 (a) and 15 (a) (from 0:00 to 5:00 and 20:00 to 23:00), because the capacity of the fuel cell in February was large as compared to that in August. Because the water electrolyzer operated using the surplus electric power of the photovoltaics, as

shown in Figs. 14 (b) and 15 (b), the duration of operation of the water electrolyzer in August was longer than in February.

As shown in Figs. 14 (c) and 15 (c), the COP of the heat pump in February was low as compared to that in August because the outside air temperature in February was lower. Although the COP of the heat pump increased with the load factor, the influence of the outside air temperature was stronger than that of the COP, as shown in Fig. 8.

According to this analysis, there was almost no difference in the operation method of the distributed system and the central system caused by seasonal changes.

4.4 Plan of equipment capacity

For year-long operation of the system, the capacity of equipment needs to be fixed. Therefore, capacities of the fuel cell and the water electrolyzer, the maximum capacity of the heat pump and the maximum area of the solar cell were determined based on the results of Figs. 11 and 12 water electrolyzer heat pump. Although the capacities of the fuel cell, the water electrolyzer, and the heat pump were almost the same for both the distributed system and the central system, the area of the solar cell could be reduced by 12% in the distributed system as compared to the central system based on the data shown in Fig. 12 (a).

5. Conclusions

In this paper, the operation method of an energy-independent microgrid was investigated based on the electric power and thermal energy income and output. A GA was used to optimize the analysis, and this paper described how the GA was applied to the operation planning in detail. Moreover, the method of operation was evaluated for the central system, which had one set of fuel cells, water electrolyzers, and heat pumps, and the distributed system, which had pieces of equipment that were distributed and arranged. The following conclusions were obtained from analyzing the operation plan of the green microgrid in a residence in a cold district:

(1) The operation method and capacity of the fuel cell, the water electrolyzer, the heat pump, and the solar cell of a representative day for each month and at each sampling time of the representative

day were clarified in detail. Furthermore, the differences between a central system and a distributed system were described in detail.

(2) The area of the total solar cell of the distributed system was smaller than the central system during the period of the mid-term of the second half to winter. Therefore, a distributed system would be more suitable due to the higher operation efficiency as compared to a central system.

(3) Because the load factor of the fuel cell was low in the summer season as the heat pump consumed less power, the efficiency of the fuel cell of the distributed system during the summer season was high compared to the central system. Therefore, the fuel cell of the distributed system could operate with a higher power generation efficiency as compared to the central system with a large capacity.

(4) Although there was almost no difference between the total capacities of the fuel cell, the water electrolyzer, or the heat pump in the distributed system and the central system, however, the area of a solar cell reduces the distributed system 12% compared with the central system.

It is future study to investigate the transient response characteristics and voltage control of electric power of a green-microgrid. The equipment cost of the proposed green microgrid is high. However, the component engineering of the system may develop largely in the future. Development of the green-microgrid is strongly related to economical efficiency, environmental impact, and expectation for green energy.

Nomenclature

COP	:	Coefficient of performance of the heat pump	
E	:	Power	[W]
E_{needs}	:	Power demand	[W]
G_g	:	Generated gas volume	[g/s]
H	:	Heat	[W]
H_{needs}	:	Heat demand	[W]
$I_{EL,c}$	:	Current required to turn on electricity	[A]

$I_{EL,g}$: Current contributed by electrolysis [A]

L_f : Load factor [%]

N : The number of pieces of equipment

P : Pressure [MPa]

P_∞ : Atmospheric pressure [MPa]

$Q_{H_2,ST}$: The amount of stored hydrogen [W]

t : Sample time [Hour]

U_∞ : Volume flow at atmosphere [MPa]

V_{EL} : Bath voltage [V]

Greek Symbols

α, β, χ : Load rate of a distributed fuel cell

ξ, ψ, ζ : Power input rate of a distributed electrolyzer

η : Efficiency

η_{dc} : Efficiency of a DC-DC converter

η_{ELe} Potential efficiency

η_{ELi} Current efficiency

η_{it} : Efficiency of an inverter

Subscripts

BW : Blower

CP : Compressor

EL : Electrolyzer

FC : Fuel cell

FC_e : Power output of a fuel cell

FC_h : Heat output of a fuel cell

HP : Heat pump

HST : Heat storage

PV : Photovoltaics

th : Theoretical

Acknowledgements

This work was partially supported by a Grant-in-Aid for the Fundamental Research Developing Association Shipbuilding Offshore, 2010. We appreciate the support of this research by the REDAS.

References

[1] Shahnia F., Majumder R., Ghosh A., Ledwich G., Zare F. Operation and control of a hybrid microgrid containing unbalanced and nonlinear loads. Electric Power Systems Research, 2010, 80(8): 954-965.

[2] El-Sharkh M.Y., Rahman A., Alam M.S. Short term scheduling of multiple grid-parallel PEM fuel cells for microgrid applications. Int J Hydrogen Energy, 2010;35(20):11099-11106.

[3] Zhang Z., Huang X., Jiang J., Wu B. A load-sharing control scheme for a microgrid with a fixed frequency inverter. Electric Power Systems Research. 2010;80(3):311-317.

[4] Molina M.G., Mercado P.E. Stabilization and control of tie-line power flow of microgrid including wind generation by distributed energy storage. Int J Hydrogen Energy, 2010;35(11):5827-5833.

[5] San Martin, J.I., et al., Influence of the rated power in the performance of different proton exchange membrane (PEM) fuel cells. Energy, 2010. 35(5): p. 1898-1907.

[6] Houwing, M., et al., Uncertainties in the design and operation of distributed energy resources: The case of micro-CHP systems. Energy, 2008. 33(10): p. 1518-1536.

[7] Jiayi H., Chuanwen J., Rong X. A review on distributed energy resources and microgrid. Renewable and Sustainable Energy Reviews, 2008;12(9):2472-2483.

[8] A.D. Hawkes, M.A. Leach. Modeling high level system design and unit commitment for a microgrid. Applied Energy, 2009;86(7-8):1253-1265.

[9] Schicktanz, M.D., J. Wapler, and H.M. Henning, Primary energy and economic analysis of combined heating, cooling and power systems. Energy, 2011. 36(1): p. 575-585.

[10] Sanseverino, E.R., et al., An execution, monitoring and replanning approach for optimal energy management in microgrids. Energy, 2011. 36(5): p. 3429-3436.

[11] Niknam, T., H.Z. Meymand, and H.D. Mojarrad, An efficient algorithm for multi-objective optimal operation management of distribution network considering fuel cell power plants. Energy, 2011. 36(1): p. 119-132.

[12] Rosen, M.A., Advances in hydrogen production by thermochemical water decomposition: A review. Energy, 2010. 35(2): p. 1068-1076.

[13] Kamel, R.M., A. Chaouachi, and K. Nagasaka, Wind power smoothing using fuzzy logic pitch controller and energy capacitor system for improvement Micro-Grid performance in islanding mode. Energy, 2010. 35(5): p. 2119-2129.

[14] Bayod-Rújula, A.A., Future development of the electricity systems with distributed generation. Energy, 2009. 34(3): p. 377-383.

[15] Siddiqui, A.S. and C. Marnay, Distributed generation investment by a microgrid under uncertainty. Energy, 2008. 33(12): p. 1729-1737.

[16] Bailey, R.A., Net energy analyses of eight technologies to provide domestic hot water heat. Energy, 1981. 6(10): p. 983-997.

[17] Verda, V. and F. Colella, Primary energy savings through thermal storage in district heating networks. Energy. In Press, Corrected Proof.

[18] Sitthidet V., Issarachai N., Somyot K. Application of electrolyzer system to enhance frequency stabilization effect of microturbine in a microgrid system. Int J Hydrogen Energy, 2009; 34(17):7131-7142.

[19] Gibson T. L., Kelly N. A. Optimization of solar powered hydrogen production using photovoltaic electrolysis devices. Int J Hydrogen Energy, 2008;33(21):5931-5940.

[20] Diéguez P.M., Sanchis A. U. P., Sopena C., Guelbenzu E., Gandía L.M. Thermal performance of a commercial alkaline water electrolyzer: Experimental study and mathematical modeling. Int J Hydrogen Energy, 2008;33(24):7338-7354.

[21] Bilgen E. Solar hydrogen from photovoltaic-electrolyzer systems. Energy Conversion and Management, 2001;42(9):1047-1057.

[22] Clúa J. G. G., Mantz R. J., Battista H. Hybrid control of a photovoltaic-hydrogen energy system. Int J Hydrogen Energy, 2008;33(13):3455-3459:

[23] Hancock Jr. O. G. A photovoltaic-powered water electrolyzer: its performance and economics. Int J Hydrogen Energy, 1986;11(3):153-160.

[24] Kelly N. A., Gibson T. L., Ouwerkerk D. B. A solar-powered, high-efficiency hydrogen fueling system using high-pressure electrolysis of water: Design and initial results. Int J Hydrogen Energy, 2008;33(11):2747-2764.

[25] Ganguly A., Misra D., Ghosh S. Modeling and analysis of solar photovoltaic-electrolyzer-fuel cell hybrid power system integrated with a floriculture greenhouse. Energy and Buildings, 2010;42(11); 2036-2043.

[26] Chun-Hua L., Xin-Jian Z., Guang-Yi C., Sheng S., Ming-Ruo H. Dynamic modeling and sizing optimization of stand-alone photovoltaic power systems using hybrid energy storage technology. Renewable Energy, 2009;34(3):815-826.

[27] Hwang J.J., Lai L.K., Wu W., Chang W.R. Dynamic modeling of a photovoltaic hydrogen fuel cell hybrid system. Int J Hydrogen Energy, 2009;34(23):9531-9542.

[28] Thomas L. Gibson, Nelson A. Kelly, Optimization of solar powered hydrogen production using photovoltaic electrolysis devices. Int J Hydrogen Energy, 2008;33(21): 5931-5940.

[29] Tokyo gas Co., Ltd, http://www.tokyo-gas.co.jp/index_e.html, 2011

[30] Yasuda I. Development of a hydrogen production technology for fuel cells. http://www.iae.or.jp/publish/kihou/28-2/04.html, 2005. in Japanese.

[31] Rengarajan B., Natarajan S., Subramanyan V., Subbiah R., Swaminathan M., Ganapathy S., et al. Development and performance evaluation of proton exchange membrane (PEM) based hydrogen generator for portable applications. Int J Hydrogen Energy, 2011;36(2): 1399-1403.

[32] Narita K., The research on unused energy of the cold region city and utilization for the district heat and cooling. Ph. D. thesis, Hokkaido University, Sapporo; 1996.

[33] The past meteorological data, The Meteorological Agency, search. http://www.data.jma.go.jp/obd/stats/etrn/index.php

[34] NEDO Technical information data base, Standard meteorology and solar radiation data (METPV-3), http://www.nedo.go.jp/database/index.html, 2009.

Math formulae

$$\left(\sum_{i=1}^{N_{FC}} E_{FC,i,t}\right)\cdot\eta_{dc1}\cdot\eta_{it1}+\left(\sum_{j=1}^{N_{PV}} E_{PV,j,t}\right)\cdot\eta_{dc2}\cdot\eta_{it2} = E_{needs,t}+\sum_{k=1}^{N_{EL}} E_{EL,k,t}+\sum_{l=1}^{N_{HP}} E_{HP,l,t}+\sum_{m=1}^{N_{CP}} E_{CP,m,t}+\sum_{n=1}^{N_{BW}} E_{BW,n,t} \quad (1)$$

$$\sum_{i=1}^{N_{FC}} H_{FC,i,t}+\sum_{j=1}^{N_{HP}} H_{HP,j,t}+H_{HST,t-1}\cdot\eta_{HST,out}=H_{needs,t}+H_{HST,t}\cdot\eta_{HST,in} \quad (2)$$

$$\eta_{FCe}=-0.002347\cdot L_f{}^2+0.3534\cdot L_f+29.01 \quad (3)$$

$$\eta_{FCh}=-0.0010893\cdot L_f{}^2+0.239\cdot L_f+40.54 \quad (4)$$

$$\eta_{ELe}=V_{EL,th}/V_{EL} \quad (5)$$

$$\eta_{ELi}=I_{EL,g}/I_{EL,c}=G_g/G_{g,th} \quad (6)$$

$$\eta_{EL}=\eta_{ELe}\cdot\eta_{ELi} \quad (7)$$

$$\eta_{EL}=-0.00005563\cdot L_f{}^3+0.009413\cdot L_f{}^2-0.6617\cdot L_f+97.31 \quad (8)$$

$$E_{CP,H_2,t}=P_\infty\cdot U_{\infty,t}\cdot\ln(P_{CP,H_2}/P_\infty)/\eta_{CP} \quad (9)$$

$$\sum_{i=1}^{N_{FC}} E_{FC,i,t}=\alpha_t\cdot E_{FC,1,t}+\beta_t\cdot E_{FC,2,t}+\chi_t\cdot E_{FC,3,t} \quad (10)$$

$$\sum_{k=1}^{N_{EL}} E_{EL,k,t}=\xi_t\cdot E_{EL,1,t}+\psi_t\cdot E_{EL,2,t}+\zeta_t\cdot E_{EL,3,t} \quad (11)$$

$$\alpha_t+\beta_t+\chi_t=1 \quad (12)$$

$$\xi_t+\psi_t+\zeta_t=1 \quad (13)$$

$$COP_{HP,16℃}=0.00000310\cdot L_f{}^3-0.000933\cdot L_f{}^2+0.0935\cdot L_f+1.012 \quad (14)$$

$$\left|Q_{H_2,ST,0}-Q_{H_2,ST,23}\right|\rightarrow \text{minimize} \qquad \text{where,} \quad Q_{H_2,ST,0}\geq Q_{H_2,ST,23} \quad (15)$$

Captions

Fig. 1 Proposed microgrid

Fig. 2 Outline of the green microgrid (distributed system)

Fig. 3 Characteristics of the PEFC and water electrolyzer

(a) Efficiency of the PEFC

(b) Efficiency of the water electrolyzer

Fig. 4 Chromosome model using a GA

Fig. 5 Power and heat demand model in Sapporo, Japan

(a) Power

(b) Heat

Fig. 6 Meteorological conditions

(a) Outside air temperature

(b) Solar insolation on sloped boad inclined at an angle of 30 degrees in the southern direction

Fig. 7 Total amount of insolation of a representative day for each month

Fig. 8 COP of the heat pump

Fig. 9 The flow of analysis using a GA

Fig. 10 The flow of analysis to optimize the capacity of each piece of equipment

Fig. 11 Analysis results for monthly system operation (1)

(a) Fuel cell

(b) Water electrolyzer

(c) Amount of hydrogen stored

Fig. 12 Analysis results for monthly system operation (2)

(a) Total area of solar cells

(b) Total capacity of heat pump

Fig. 13 The average monthly efficiency of the fuel cell and the water electrolyzer in the central system and the distributed system

Fig. 14 Analysis results of the fuel cell, the water electrolyzer and the heat pump operating daily in the distributed system

(a) Average operational efficiency of the fuel cell

(b) Average operational efficiency of the water electrolyzer

(c) Average operational COP of the heat pump

Fig. 15 Analysis results of the fuel cell, the water electrolyzer and the heat pump operating daily in the central system

(a) Efficiency of the fuel cell

(b) Efficiency of water electrolyzer

(c) Average operational COP of the heat pump

Table 1 Specifications of each component

Table 2 Computation equations used for analysis

Table 3 Parameters of the GA

Fig. 1 Proposed microgrid

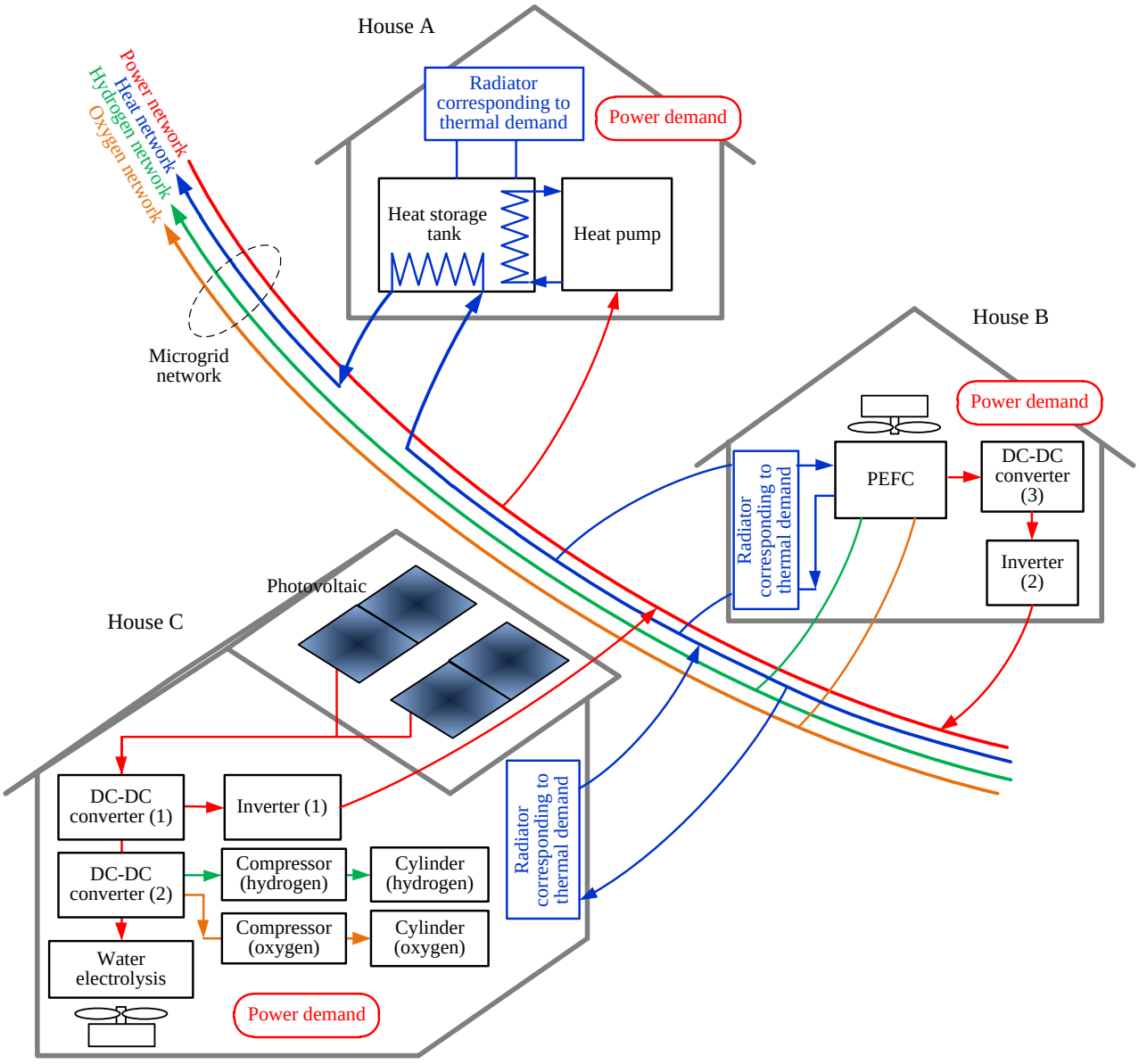

Fig. 2 Outline of the green microgrid (distributed system)

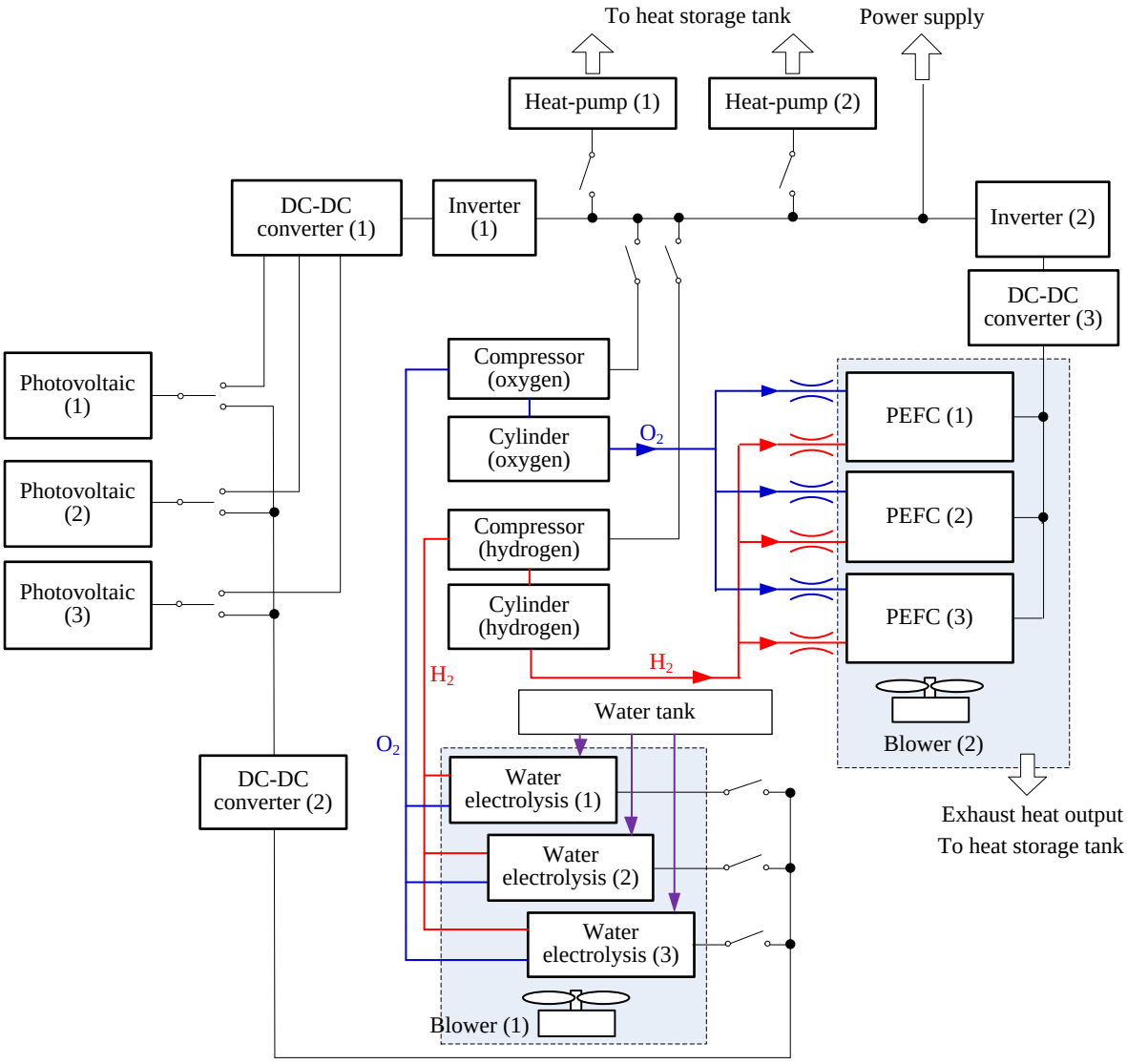

(a) Power system

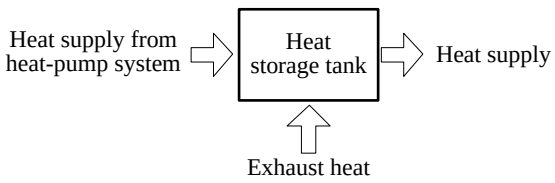

(b) Heat system

Fig. 3 Characteristics of the PEFC and water electrolyzer

(a) Efficiency of the PEFC

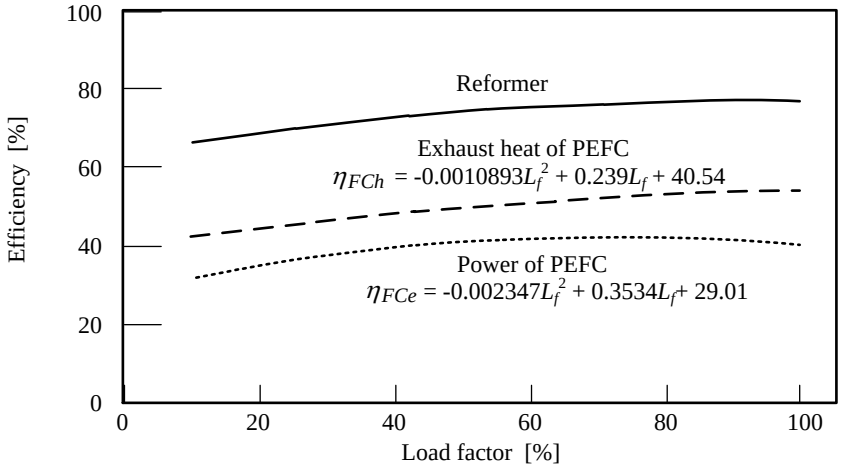

(b) Efficiency of the water electrolyzer

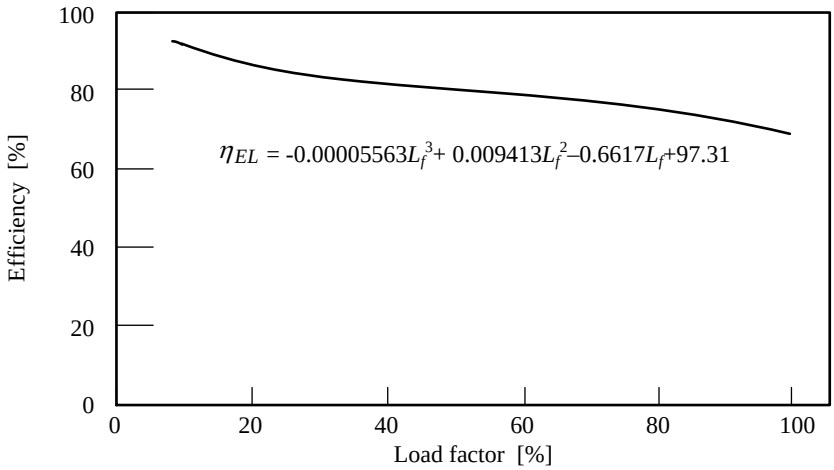

Fig. 4 Chromosome model using a GA

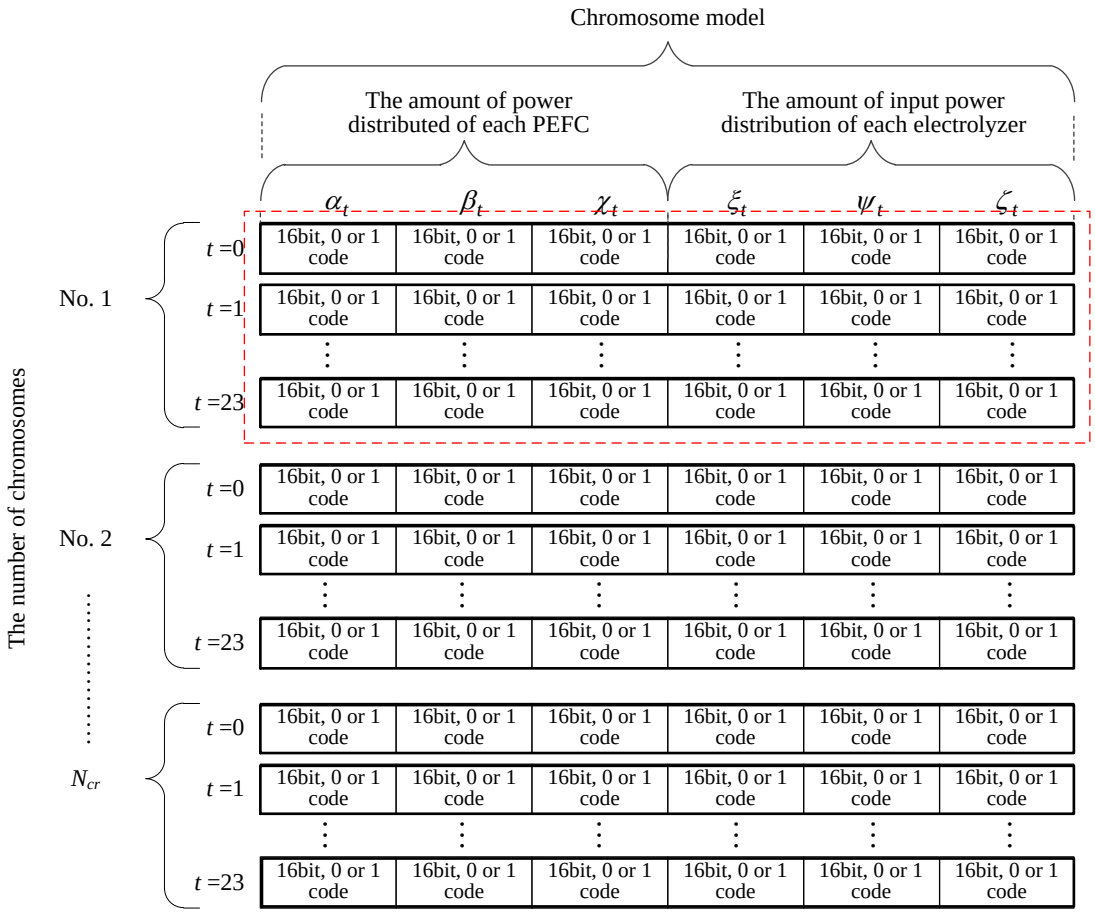

Fig. 5 Power and heat demand model in Sapporo, Japan

(a) Power

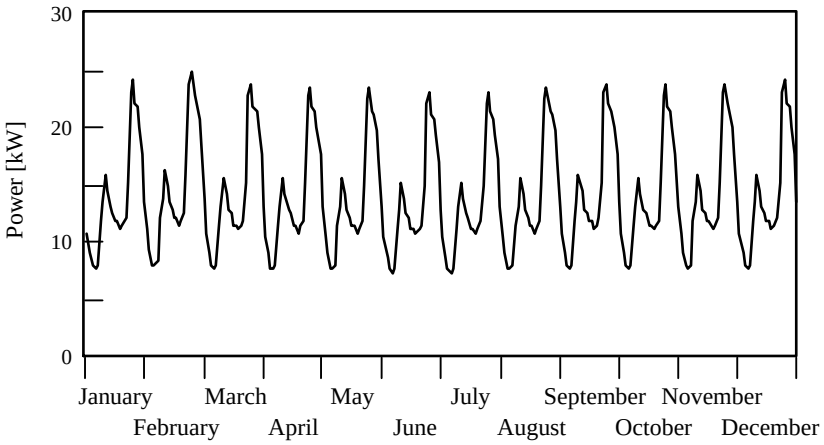

(b) Heat

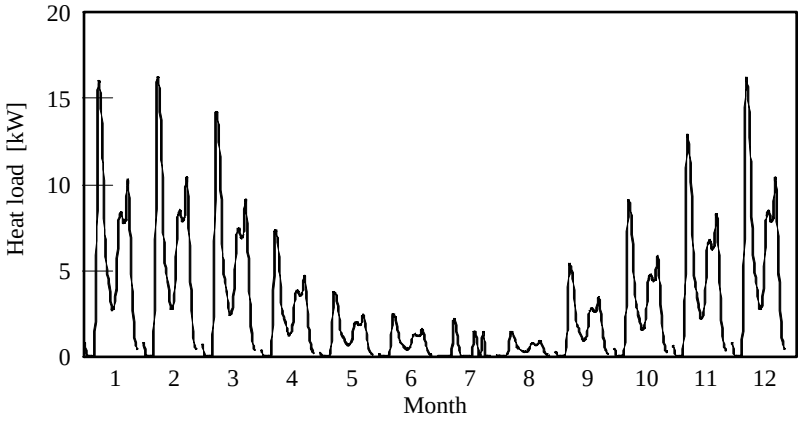

Fig. 6 Meteorological conditions

(a) Outside air temperature

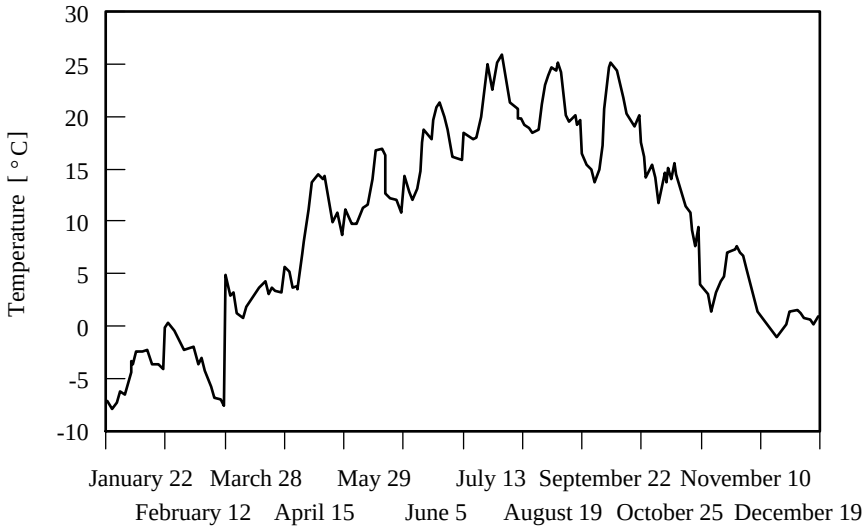

(b) Solar insolation on sloped boad inclined at an angle of 30 degrees in the southern direction

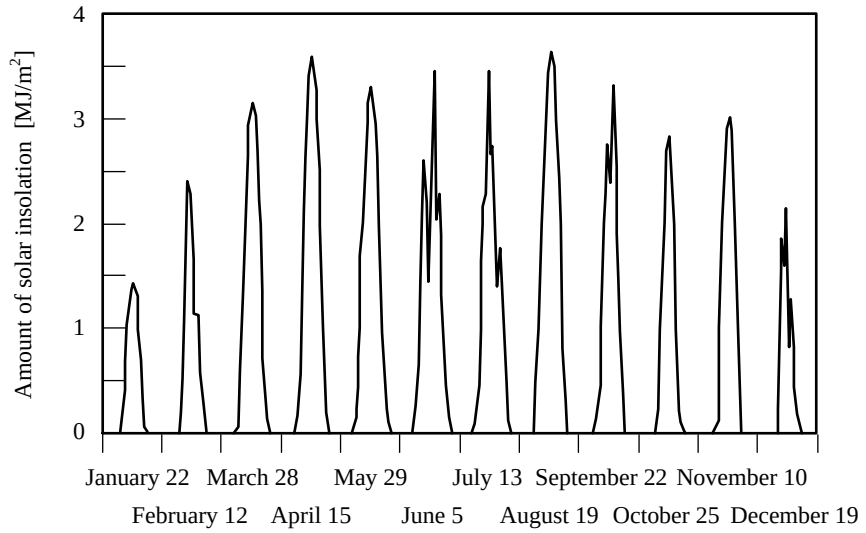

Fig. 7 Total amount of insolation of a representative day for each month

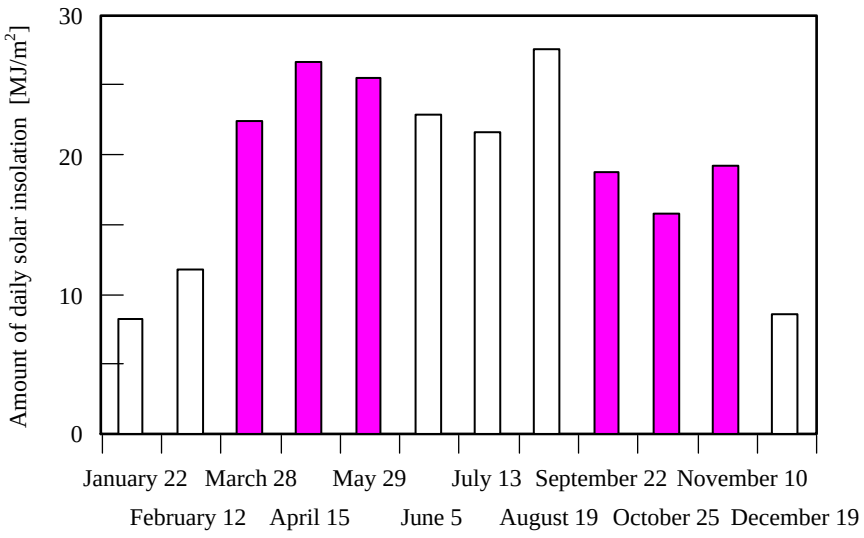

Fig. 8 COP of the heat pump

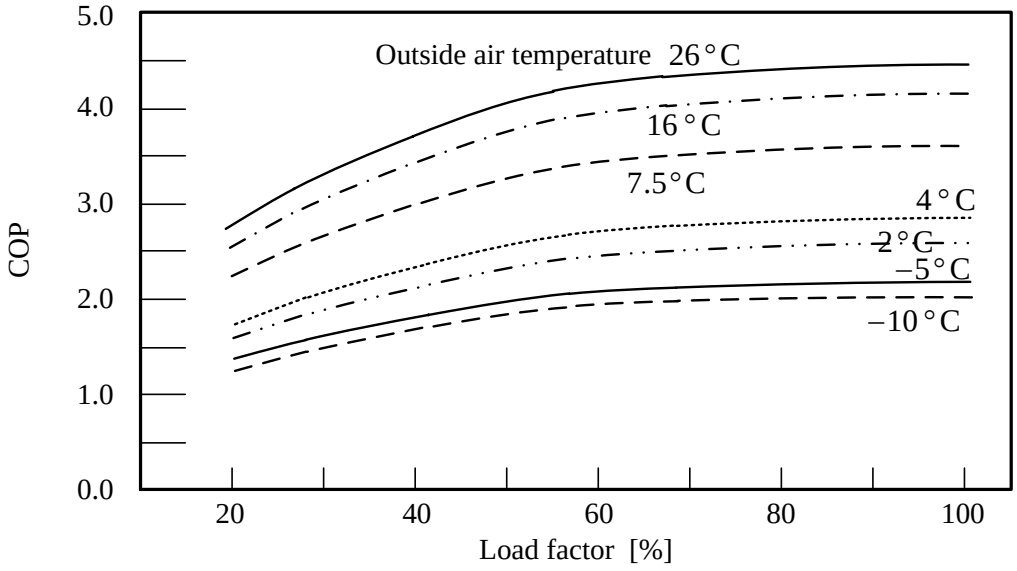

Fig. 9 The flow of analysis using a GA

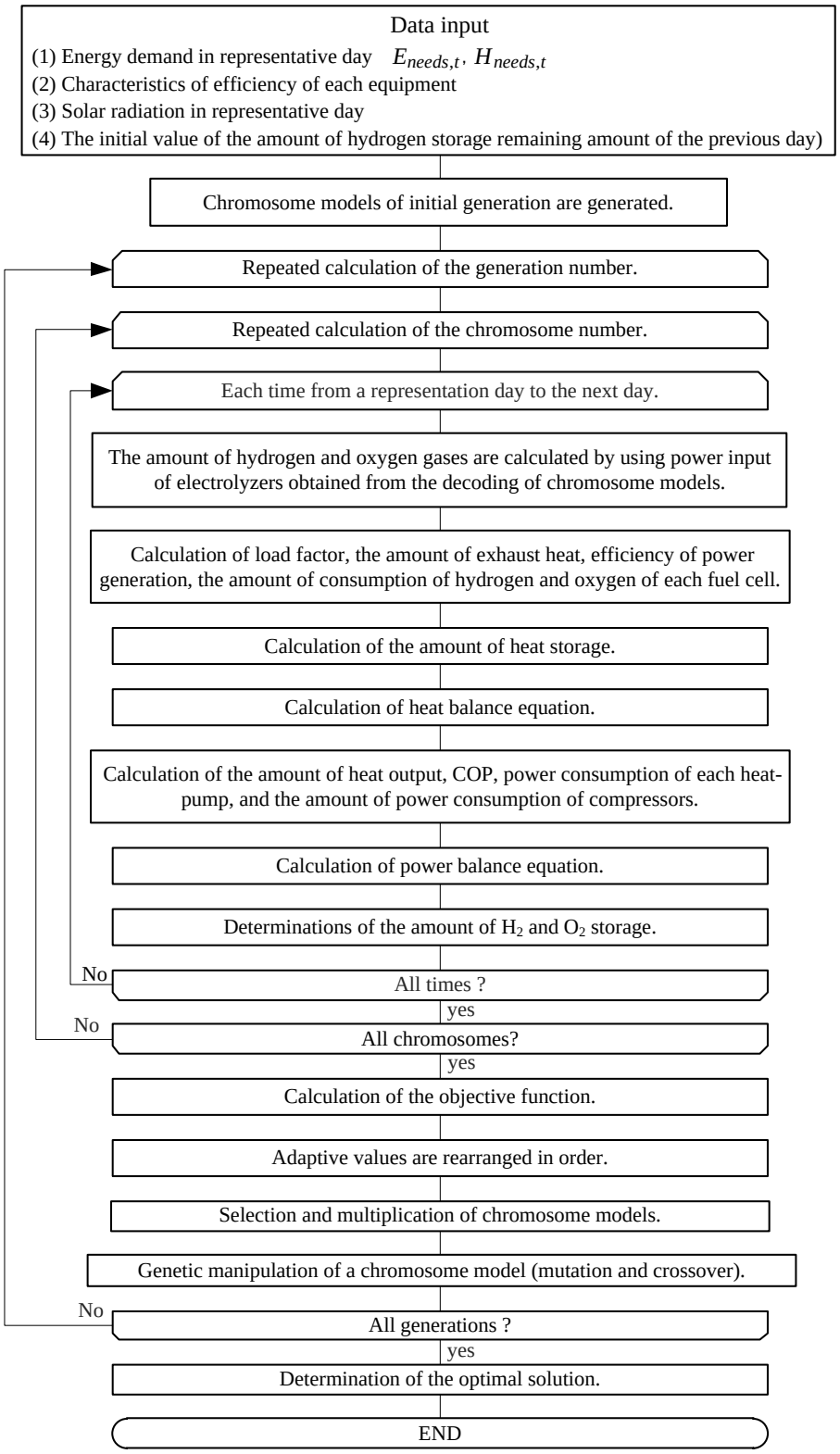

Fig. 10 The flow of analysis to optimize the capacity of each piece of equipment

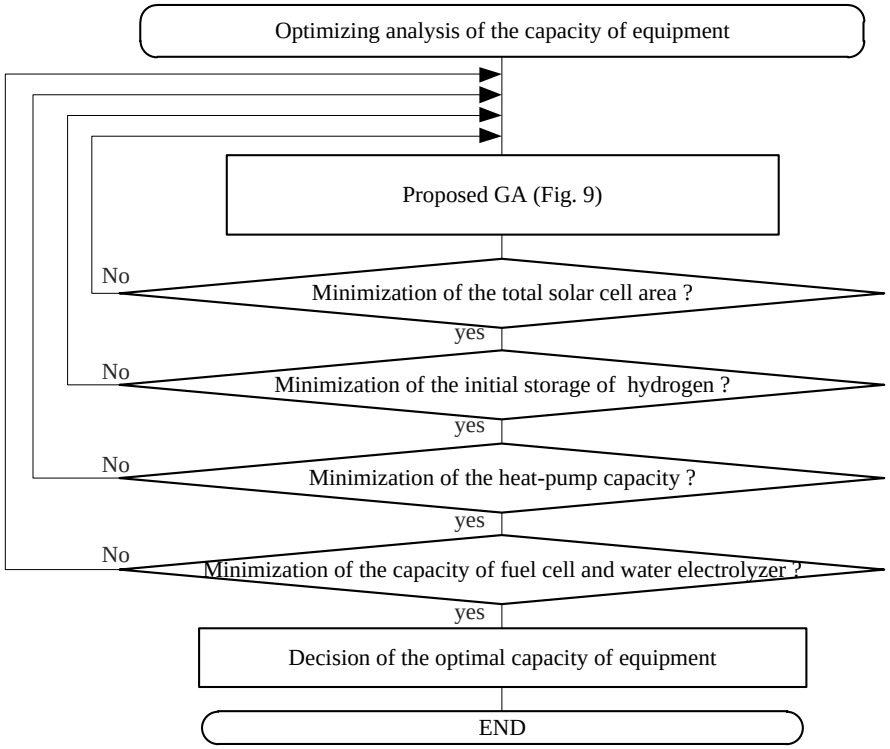

Fig. 11 Analysis results for monthly system operation (1)

(a) Fuel cell

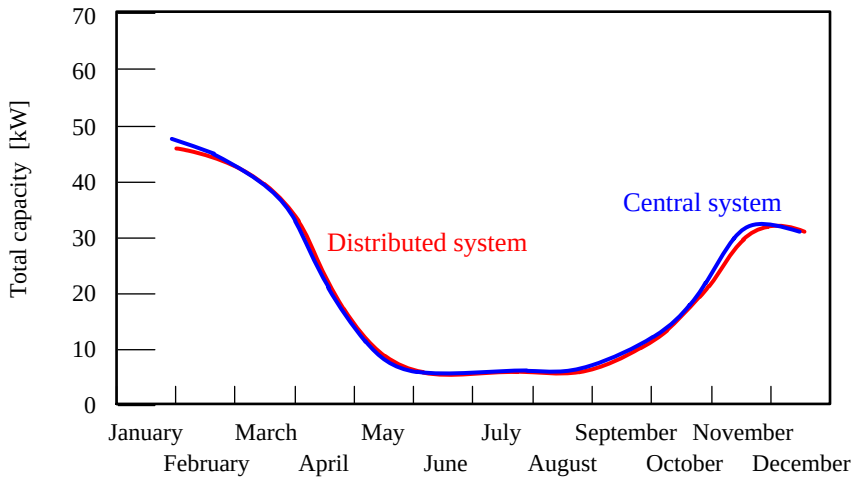

(b) Water electrolyzer

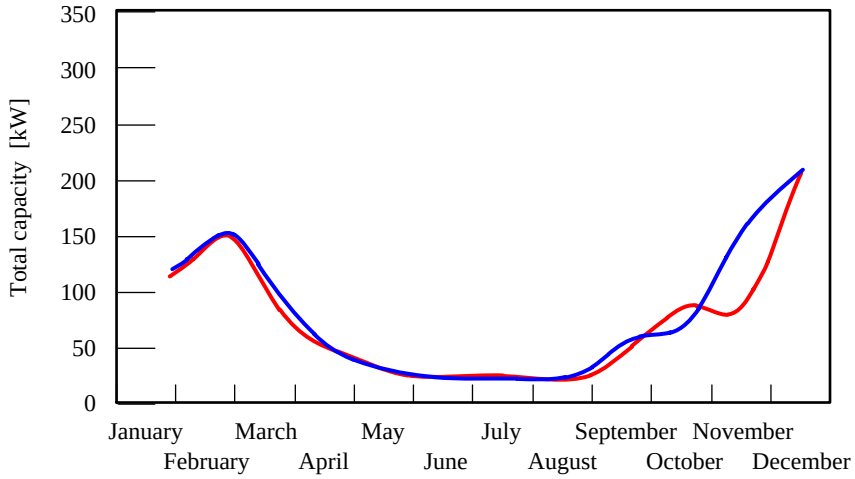

(c) Amount of hydrogen stored

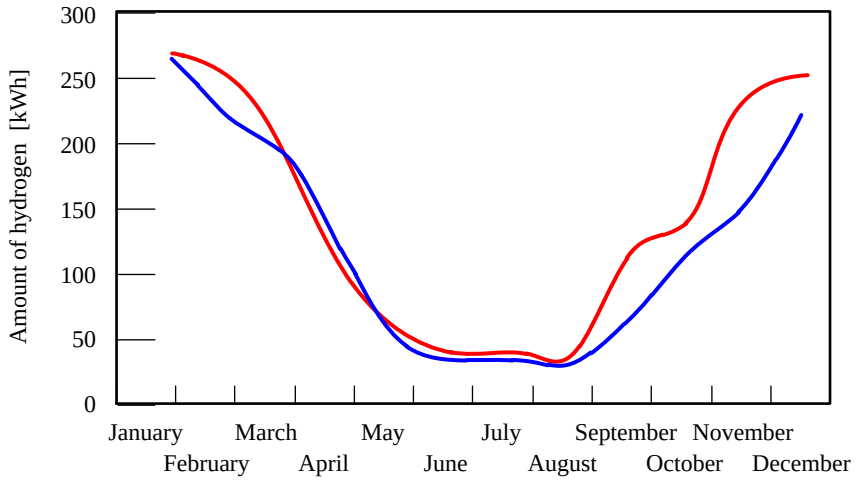

Fig. 12 Analysis results for monthly system operation (2)

(a) Total area of solar cells

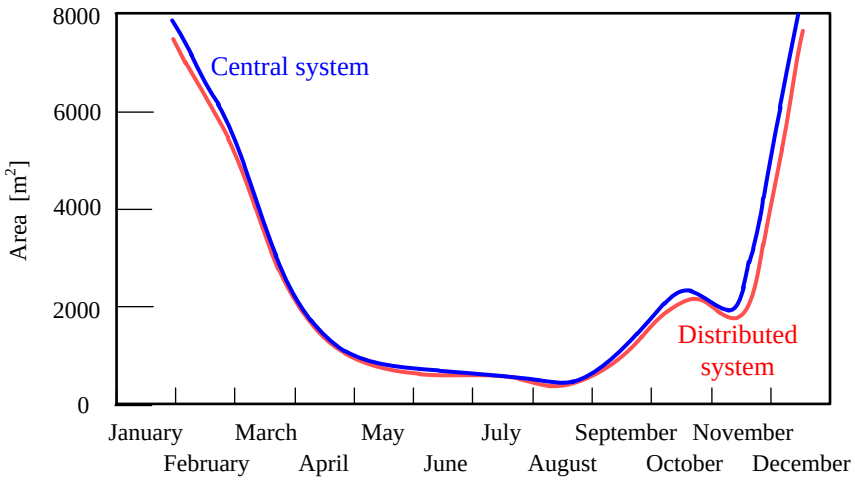

(b) Total capacity of heat pump

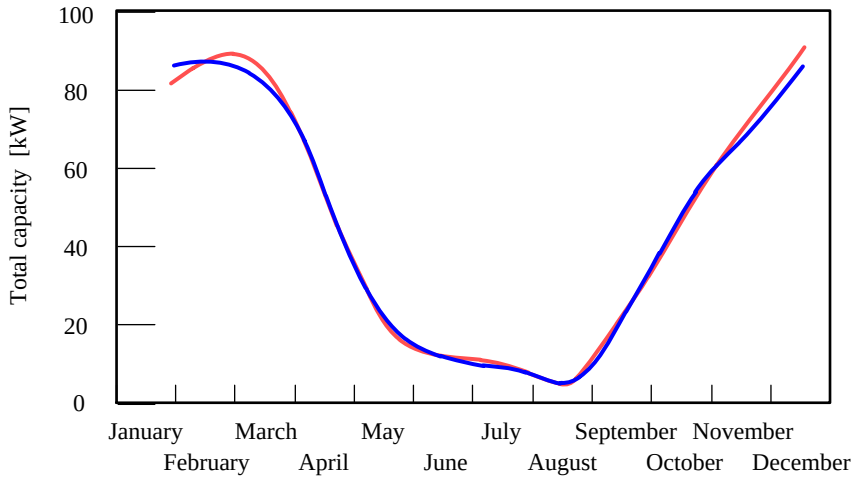

Fig. 13 The average monthly efficiency of the fuel cell and the water electrolyzer in the central system and the distributed system

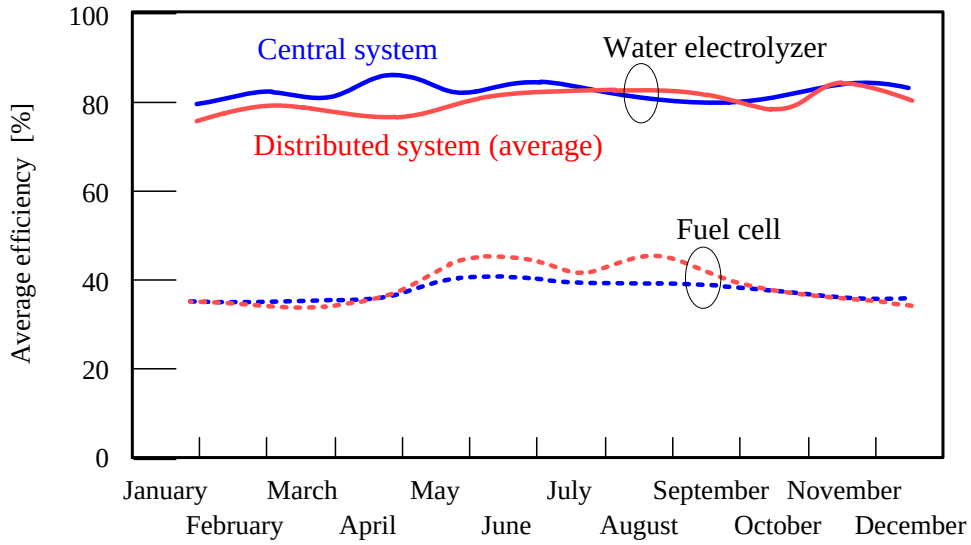

Fig. 14　Analysis results of the fuel cell, the water electrolyzer and the heat pump operating daily in the distributed system

(a) Average operational efficiency of the fuel cell

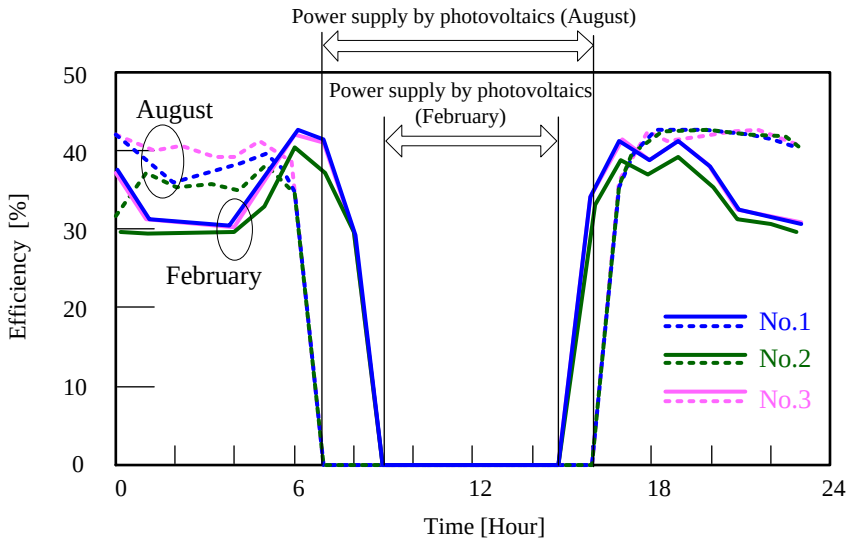

(b) Average operational efficiency of the water electrolyzer

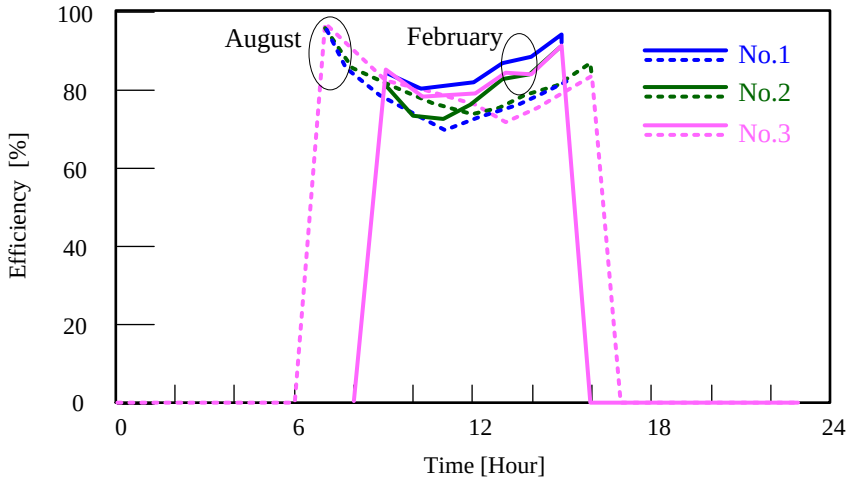

(c) Average operational COP of the heat pump

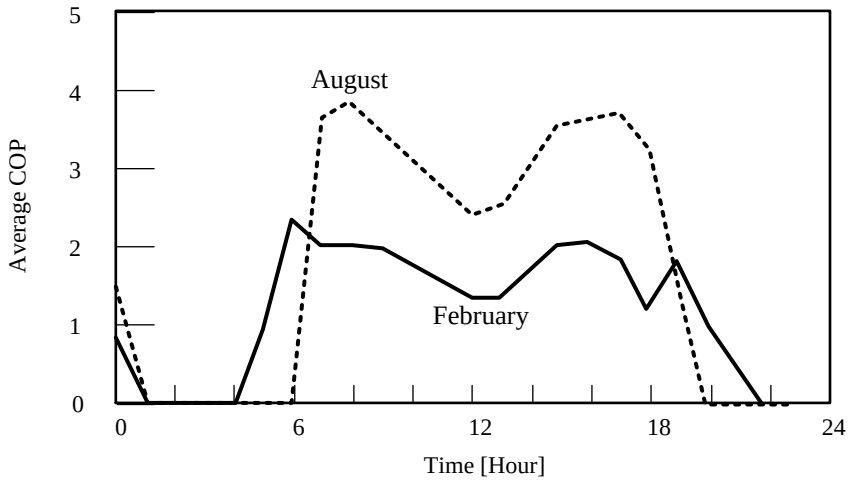

Fig. 15　Analysis results of the fuel cell, the water electrolyzer and the heat pump operating daily in the central system

(a) Efficiency of the fuel cell

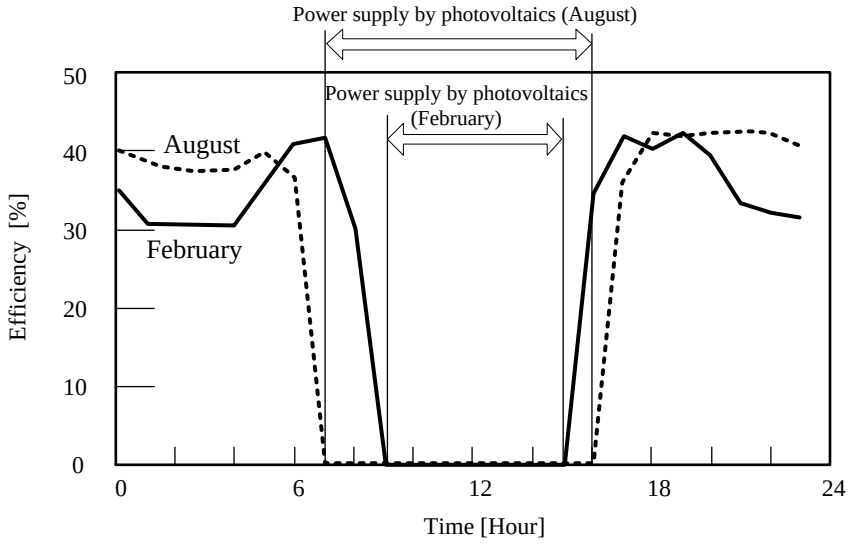

(b) Efficiency of water electrolyzer

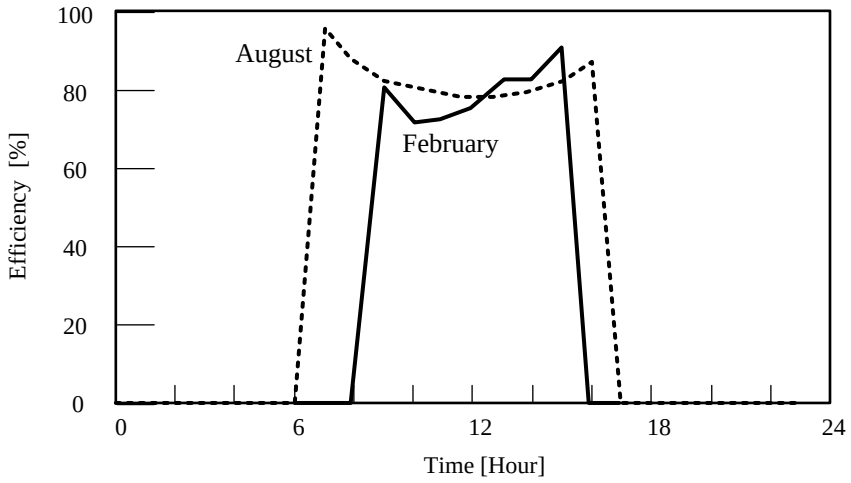

(c) Average operational COP of the heat pump

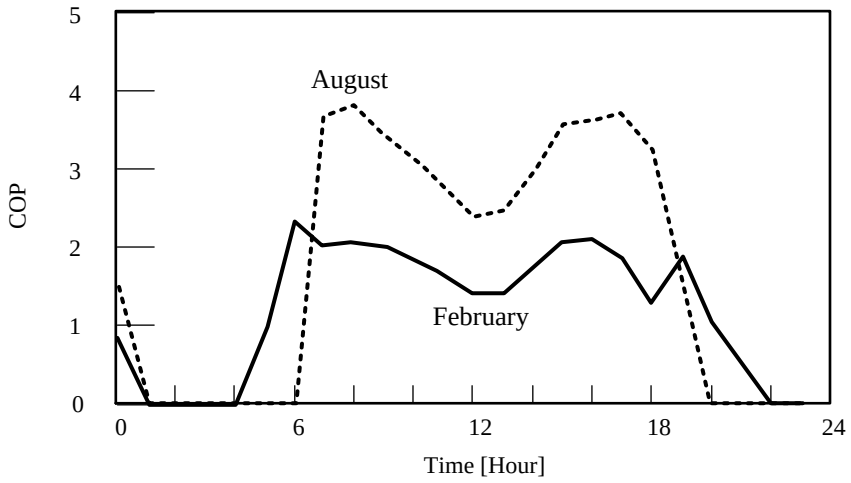

Table 1 Specifications of each component

Photovoltaics	3 sets	Heat storage tank	
Efficiency	20 %	Heat storage efficiency ($\eta_{HST,in}$)	95 %
Fuel cell (PEFC)	1 or 3 sets	Heat output efficiency ($\eta_{HST,out}$)	95 %
Efficiency	Fig. 3 (a)	Compressor (H_2 and O_2)	1 set
Electrolyzer (proton-exchange type)	1 or 3 sets	Compressed pressure (P_{CP,H_2})	1 MPa
Efficiency	Fig. 3 (b)	Efficiency (η_{CP})	60 %
Heat-pump	2 sets	Inverter ($\eta_{it,1}$, $\eta_{it,2}$)	95 %
COP	Fig. 8	DC-DC converter (η_{dc1} , η_{dc2})	95 %
		Blower (E_{BW})	50 W

Table 2 Computation equations used for analysis

1. In the case of $H_{HST,t} > H_{needs,t}$

(1) In the case of $\sum_{j=1}^{N_{PV}} E_{PV,j,t} > E_{needs,t} + \sum_{n=1}^{N_{BW}} E_{BW,n,t}$

a. $\sum_{k=1}^{N_{EL}} E_{EL,k,t} = \sum_{j=1}^{N_{PV}} E_{PV,j,t} - \left(E_{needs,t} + \sum_{n=1}^{N_{BW}} E_{BW,n,t} \right)$

b. $\sum_{i=1}^{N_{FC}} E_{FC,i,t} = 0$

c. $H_{HST,t} = H_{HST,t-1} - H_{needs,t}$

d. $Q_{H_2ST,t} = Q_{H_2ST,t-1} + \sum_{k=1}^{N_{EL}} Q_{EL,k,t} = 0$

e. $\sum_{j=1}^{N_{HP}} H_{HP,j,t} = 0$

(2) In the case of $\sum_{j=1}^{N_{PV}} E_{PV,j,t} \le E_{needs,t} + \sum_{n=1}^{N_{BW}} E_{BW,n,t}$

a. $\sum_{k=1}^{N_{EL}} E_{EL,k,t} = 0$

b. $\sum_{i=1}^{N_{FC}} E_{FC,i,t} = E_{needs,t} + \sum_{n=1}^{N_{BW}} E_{BW,n,t} - \sum_{j=1}^{N_{PV}} E_{PV,j,t}$

c. $H_{HST,t} = H_{HST,t-1} - H_{needs,t} + \sum_{i=1}^{N_{FC}} H_{FC,i,t}$

d. $Q_{H_2ST,t} = Q_{H_2ST,t-1} - \sum_{i=1}^{N_{FC}} Q_{FC,i,t} = 0$

e. $\sum_{j=1}^{N_{HP}} H_{HP,j,t} = 0$

2. In the case of $H_{HST,t} \le H_{needs,t}$

(1) In the case of $\sum_{j=1}^{N_{PV}} E_{PV,j,t} > E_{needs,t} + \sum_{n=1}^{N_{BW}} E_{BW,n,t}$

In the case of $\sum_{j=1}^{N_{HP}} H_{HP,j,t} \ge H_{needs,t} - H_{HST,t-1}$

a. In the case of $\sum_{j=1}^{N_{PV}} E_{PV,j,t} > E_{needst} + \sum_{n=1}^{N_{BW}} E_{BW,n,t} + \sum_{l=1}^{N_{HP}} E_{HP,l,t}$

- $\sum_{k=1}^{N_{EL}} E_{EL,k,t} = \sum_{j=1}^{N_{PV}} E_{PV,j,t} - \left(E_{needs,t} + \sum_{n=1}^{N_{BW}} E_{BW,n,t} + \sum_{l=1}^{N_{HP}} E_{HP,l,t} \right)$
- $\sum_{i=1}^{N_{FC}} E_{FC,i,t} = 0$
- $H_{HST,t} = 0$
- $Q_{H_2ST,t} = Q_{H_2ST,t-1} - \sum_{k=1}^{N_{EL}} Q_{EL,k,t}$

b. In the case of $\sum_{j=1}^{N_{PV}} E_{PV,j,t} \le E_{needs,t} + \sum_{n=1}^{N_{BW}} E_{BW,n,t} + \sum_{l=1}^{N_{HP}} E_{HP,l,t}$

- $\sum_{k=1}^{N_{EL}} E_{EL,k,t} = 0$
- $\sum_{i=1}^{N_{FC}} E_{FC,i,t} = E_{needst} + \sum_{n=1}^{N_{BW}} E_{BW,n,t} + \sum_{l=1}^{N_{HP}} E_{HP,l,t} - \sum_{j=1}^{N_{PV}} E_{PV,j,t}$
- $H_{HST,t} = \sum_{i=1}^{N_{FC}} H_{FC,i,t}$
- $Q_{H_2ST,t} = Q_{H_2ST,t-1} - \sum_{i=1}^{N_{FC}} Q_{FC,i,t}$

(2) In the case of $\sum_{j=1}^{N_{PV}} E_{PV,j,t} \le E_{needs,t} + \sum_{n=1}^{N_{BW}} E_{BW,n,t}$

a. $\sum_{j=1}^{N_{HP}} H_{HP,j,t} = H_{needs,t} - H_{HST,t-1}$

b. $\sum_{i=1}^{N_{FC}} E_{FC,i,t} = E_{needst} + \sum_{n=1}^{N_{BW}} E_{BW,n,t} + \sum_{l=1}^{N_{HP}} E_{HP,l,t} - \sum_{j=1}^{N_{PV}} E_{PV,j,t}$

c. $\sum_{k=1}^{N_{EL}} E_{EL,k,t} = 0$

d. $H_{HST,t} = \sum_{i=1}^{N_{FC}} H_{FC,i,t}$

e. $Q_{H_2ST,t} = Q_{H_2ST,t-1} - \sum_{i=1}^{N_{FC}} Q_{FC,i,t}$

Table 3 Parameters of the GA

The number of generations	20
The number of chromosomes	10000
Probability of cross-over	50 %
Probability of mutation	80 %
Chromosome model (Individual)	Fig. 4